

Solar Photothermal Disinfection using Broadband-Light Absorbing Gold Nanoparticles and Carbon Black

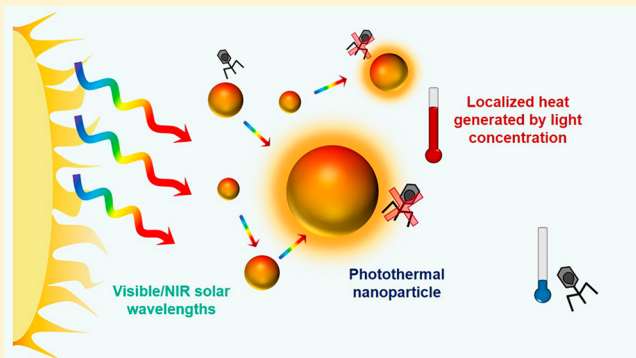
Stephanie Loeb,[†] Chuanhao Li,^{†,‡} and Jae-Hong Kim*,^{†,ID}

[†]Department of Chemical and Environmental Engineering and Nanosystems Engineering Research Center for Nanotechnology-Enabled Water Treatment (NEWT), Yale University, 17 Hillhouse Ave, New Haven, Connecticut 06511, United States

[‡]Department of Environmental Science and Engineering, Sun Yat-sen University, Guangzhou, Guangdong China

Supporting Information

ABSTRACT: A simple heat treatment, perhaps the most globally recognized point-of-use water sterilization method, is seemingly effective against all major pathogens of concern, but bulk water boiling is not energy efficient or sustainable. Herein, we present the first application of solar-to-thermal converting nanomaterials for the direct inactivation of bacteria and viruses in drinking water through the application of Au nanorods, carbon black, and Au nanorod-carbon black composite materials as light absorbers. With broad absorption bands spanning the visible and near-infrared wavelengths, at sufficient concentrations, these nanoparticles induce multiple scattering events, increasing photon absorption probability and concentrating the light within a small spatial domain, leading to localized, intense heating that inactivates microorganisms in close proximity. Moving toward practical device design, we have developed a facile silane immobilization approach to fabricate films with densely packed layers of photothermal nanomaterials. Our results suggest that upon irradiation with simulated solar light, these films can thermally inactivate bacteria and viruses, as demonstrated through the inactivation of surrogate organisms *Escherichia coli* K-12, and bacteriophages MS2 and PR772.



INTRODUCTION

Worldwide, 2 billion people are reliant on a drinking water source contaminated with feces, resulting in over half a million deaths each year related to the consumption of unsafe water and preventable waterborne illnesses, with a majority of deaths caused by diarrheal diseases.¹ Point-of-use (POU) water disinfection is often considered the most practical solution to provide safe drinking water, especially in rural communities where centralized public water supply systems have not been implemented or have failed to sustainably function. POU treatment, if properly designed and implemented, can simplify the overall treatment process, reduce the risk of microbial recontamination, and obviate large capital infrastructure and maintenance costs.² One of the simplest options is the exposure of water in a transparent container to solar irradiation, known as solar disinfection (SODIS). Despite its widespread application, SODIS suffers from unpredictable and ineffective disinfection due to reliance on a small fraction of the solar spectrum (i.e., terrestrial UV).^{3,4} Advanced materials that can more effectively harness solar energy for POU water treatment have been extensively explored; however, current materials such as photocatalysts and photosensitizers are often cost-prohibitive and lack proper engineering solutions for practice in the field.⁵ A suite of other chemical treatment methods also exist, but each

requires a consumable material, and presents risks related to the promotion of persistent antibiotic resistance and formation of disinfection byproducts.

Water disinfection by boiling is a traditional, ubiquitous method with proven direct positive health outcomes.⁶ The direct use of solar energy to thermally inactivate pathogens in water would be more desirable than heating and pasteurizing large volumes of water by burning a consumable fuel. However, water has a high heat capacity and is a poor absorber of solar irradiation. Consequently, the temperatures necessary to achieve synergistic inactivation by heat and sunlight are rarely achieved in SODIS practice.⁷ Materials that have the ability to passively generate high temperatures from exposure to light and transfer this heat to target pathogens might be therefore instrumental in developing a new technology that directly utilizes solar energy for disinfection via heating. Several photothermal materials, including carbon^{8–11} and metallic nanoparticles^{12,13} have the capability to localize heat through efficient absorption of incident photons. Noble metals in

Received: August 29, 2017

Revised: October 31, 2017

Accepted: December 1, 2017

Published: December 14, 2017

nanoparticle architectures (e.g., Au, Ag, Cu, Al) exhibit photothermal properties through surface plasmon resonance (SPR) with resonant photons in the visible and near-infrared (NIR) regions,^{14–16} wavelengths which account for ~90% of the solar spectrum. Some past studies have explored the use of SPR photothermal materials to control pathogens, mostly employing high-intensity laser light sources for photodynamic therapy and biofilm control applications.^{17–21} Under high intensity radiation, experiments have shown that, at the nanoparticle–water interface, SPR materials can superheat water to its spinodal decomposition temperature (321 °C).²²

Under noncoherent, low-intensity radiation, that is, solar light conditions, these photothermal nanoparticles were initially thought to simply serve as volumetric absorbers and conductors of heat to the surrounding medium, without creating extreme temperatures.²³ However, more recent studies have achieved highly localized heating using photothermal nanoparticles under only solar irradiation. In one of the first studies to show this effect, Neumann et al.²⁴ were able to generate steam in 10s of seconds by irradiating a suspension of either Au/SiO₂ nanoshells or carbon black, with focused sunlight while controlling bulk water temperature below 7 °C. For the carbon black suspension, a majority (~82%) of the solar energy absorbed was directed toward steam generation instead of bulk water heating, enabling the first demonstration of solar photothermal distillation.²⁴ This heating is shown to result from the trapping of photons and overall much higher absorption than predicted by conventional theory.²⁵ Since steam production under low intensity solar radiation requires the cumulative effect of multiple nanoparticles,²⁶ the accurate characterization of particle surface temperature in these conditions has not yet been reported, although temperatures above 100 °C are evidently achieved.

We herein hypothesize that intense localized heating through light concentration by photothermal materials, generated under solar irradiation, can inactivate bacteria and viruses without substantially raising the bulk temperature of the water. This process is a reinvention of disinfection by boiling water; the need for a consumable fuel is eliminated, replaced by renewable and ubiquitous solar energy and a reusable catalytic material. In this proof-of-concept study, we examine the photothermal inactivation of common water-borne pathogen surrogates bacteriophage MS2, and *E. coli* K-12, as well as the adenovirus surrogate DNA bacteriophage PR772 to more fully represent the broad diversity of viral pathogenic species. Inactivation kinetics for each surrogate are established in the presence of Au nanocubes, Au nanorods, and carbon black photothermal nanoparticles under simulated solar radiation. Moving toward more practical engineering solutions, photothermal surfaces are fabricated by adhering nanoparticles to glass substrates, and the inactivation capabilities of these surfaces are quantified.

MATERIALS AND METHODS

Materials. All reagents for nanoparticle synthesis were purchased from Sigma-Aldrich. Gold chloride (HAuCl₄, 99.999%) was used as a precursor for the synthesis of Au nanoparticles. Carbon black Emperor 2000 powder was supplied by Cabot Industries. This material was selected for its known photothermal properties, low cost, ease of dispersion in water, and broadband absorption at visible and NIR wavelengths. MS2 (ATCC 15597-B1) and PR772 (ATCC BAA-769-B1), *E. coli* C3000 (ATCC 15597), and *E. coli* K12 J53-1 (ATCC BAA-769) were purchased from American Type

Culture Collection (ATCC), propagated according to manufacturer's specifications and maintained as glycerol stocks at –80 °C for long-term storage.

Synthesis of Photothermal Nanomaterials. Au nanocubes and Au nanorods were synthesized using a seeded-growth method previously reported in the literature.^{27–29} Seed solutions were prepared by adding sodium borohydride (NaBH₄) into a solution of HAuCl₄ and cetyltrimethylammonium bromide (CTAB), a cationic surfactant that acts as a capping agent, controlling nanoparticle growth and preventing aggregation. Nanocube synthesis was achieved through slow reduction of HAuCl₄ by ascorbic acid in the presence of the seed solution. This method was modified to produce Au nanorods by the addition of AgNO₃, which directionally completes for growth sites with HAuCl₄, promoting longitudinal growth, resulting in the formation of nanorods. Detailed synthesis procedures can be found in [Supporting Information \(SI\) Text S1](#). Prior to further use, Au nanoparticles were washed twice by repeated centrifugation at 6000 rpm for 1 h and resuspended in DI water (>18.2 MΩ). Molar concentrations of washed nanomaterials were determined using inductively coupled plasma-mass spectrometry (ICP-MS).³⁰ ICP-MS results were then used to create a spectrophotometric calibration using absorbance at the peak SPR wavelength allowing for rapid subsequent mass determination. ICP-MS results and UV-vis calibration curves are presented in [SI Figure S1](#). The molar concentration of carbon black was determined by weight, assuming the molar mass to be the same as carbon (12.01 g/mol).

Fabrication of Photothermal Films. To fabricate photothermal films, glass coverslips (1.5 mm thickness, 12 mm diameter, Harvard Apparatus CS12R15) were cleaned in hot pirhana solution (3:1 H₂SO₄ and H₂O₂), rinsed with DI water, dried under a stream of N₂, and heat-treated at 105 °C for 10 min. For carbon black fixation, surface silanation with 3-aminopropyltrimethylsiloxane (APTMS) was achieved by refluxing cleaned substrates for 15 min in 10 mL isopropyl alcohol (IPA), 100 μL APTMS, and 200 μL DI water. Substrates were slowly cooled in solution, rinsed in IPA, dried under a stream of N₂, and heat treated at 105 °C for 10 min. After cooling, substrates were arranged in a glass Petri-dish and drop casted with 10–12 drops of 0.45 μm-filtered 1 mg/L carbon black solution, forming a neat miniscus on the surface. After 30 min, substrates were rinsed with DI water, dried under a stream of N₂, and heat treated at 105 °C for 10 min. This process was repeated three times, on both sides of the substrate.

For Au nanorod fixation, surface silanation with 3-mercaptopropyltrimethylsiloxane (MPTMS) was achieved as described above, replacing APTMS with 100 μL MPTMS.³¹ Tightly packed, dense Au nanorod films were fabricated on MPTMS modified surfaces using an adaptation of the method by Yun et al.³² Briefly, 25 mL of twice-washed Au nanorod solution was added to a Teflon beaker and covered with 10 mL of hexanes, forming an immiscible surface layer. Next, 6 mL of ethanol was added dropwise using a syringe pump (Harvard Apparatus, PHD 2000 Infusion) at a rate of 0.6 mL/min. Ethanol enters into the underlying aqueous phase, thereby altering the dielectric constant of the medium and reducing Au nanorod surface charge. This decreases the repulsive force between particles, allowing them to pack tightly at the liquid–liquid interface and reducing the interfacial energy due to surface tension. This process traps the nanorods at the surface forming a mirror-like film as the hexane evaporates. This film is

then facilely deposited on the MPTMS modified glass substrate by slowly lifting the substrate through the film. A schematic representation of this fabrication process can be found in *SI Figure S2*. Packing density of nanorods on the surface was determined by analyzing the threshold contrast area fraction covered using ImageJ, averaged over 5 images. Layered composite carbon black and Au nanorod films were fabricated by first applying the carbon coating, treating the carbon coated glass with MPTMS, then applying a dense Au nanorod layer over top.

Material Characterizations. Shape and structure of photothermal nanomaterials were characterized using a Hitachi SU-70 scanning electron microscope (SEM) and an FEI Tecnai Osiris 200 kV tunneling electron microscope (TEM). For SEM analysis, films were prepared on 2 cm × 2 cm silicon substrates. The absorption spectra of each material was determined by UV-vis spectroscopy using a Varian Cary 50 Bio UV-visible spectrophotometer. Absorption spectra of photothermal films were measured using diffuse reflectance spectroscopy (DRS) with a UV-vis Cary 3E spectrophotometer equipped with an integrating sphere and corrected by the Kubelka-Munk equation. Hydrodynamic radius and zeta potential at pH 7.2 were determined using dynamic light scattering (DLS) with a NanoBrook omni particle sizer and phase-alternative light scattering (PALS) with a zeta potential analyzer, respectively.

Bulk Water Heating. The extent of bulk temperature rise was measured for each material at the same molar concentration of 10 μM and normalized at the same integrated optical density (OD) of 500. Optical density was determined by integrating the absorption spectra from 300 to 1000 nm. Prior to light exposure, all samples were stored in falcon tubes in an ice bath to maintain equivalent initial temperature. The same quartz vial, containing 20 mL of solution, was used for each experiment. The vial was covered with parafilm and the temperature probe was pierced through the surface of the film. The solution was left to equilibrate until it reached a temperature of 10 °C. Samples were then irradiated with light from an ABET industries solar simulator (emission spectra *SI Figure S4*), which generates light using a short arc xenon lamp directed through an AM1.5G filter. The distance between the sample and the light source was aligned to correspond to 1 sun intensity at 100 mW/cm², as measured with a PMA2140 global radiometer. Temperature increase was monitored over a 30 min period. To isolate the contribution of NIR wavelengths, the experiment was repeated with a 675 nm long pass filter (Thor Laboratories) applied to the outlet of the solar simulator. Since the 675 nm filter attenuates the intensity of transmitted wavelengths by 20%, the intensity of the light was corrected by reducing the distance between the light source and the sample when the long-pass filter was used.

Microbial Inactivation. *E. coli* C3000 and K12 J53-1 strains were used as the respective host organisms for MS2 bacteriophage and PR772 after growing for a minimum of 6 h in tryptic soy broth to reach the exponential growth phase. *E. coli* K-12, used for inactivation experiments, was grown in Lysogeny broth to an OD₆₀₀ of ~1, extracted by centrifugation at 5000 rpm for 10 min, and washed twice with phosphate buffer saline (PBS; 1 mM at pH 7.2) prior to further experiments. All equipment used during inactivation experiments were autoclave sterilized at 120 °C for 60 min and standard aseptic practices were followed throughout. Nanoparticulate suspensions were sterile filtered using 0.45 μm syringe filters.

Suspension inactivation experiments were conducted in 10 mL of PBS. Sterile Petri-dishes were positioned under the solar simulator and filled with 10 mL PBS containing ~5 × 10⁶ PFU(CFU)/mL (plaque forming units or colony forming units per mL) of the surrogate microorganism, and covered with a quartz plate to prevent vapor loss. Photothermal materials were added to achieve a final concentration of 25 μM. Solutions were then exposed to 1 sun simulated solar irradiation and the viability was monitored over the exposure time. A schematic of the inactivation experimental setup is shown in *SI Figure S6*. Bacteriophages were assayed via a soft-overlay technique as previously described.³³ Plates were incubated overnight at 37 °C, after which discretely formed viral plaques can be counted. Bacteria samples were analyzed using a standard spread-plate counting method.³⁴

The antimicrobial activity of immobilized materials was evaluated similarly. Photothermal films fabricated on glass coverslips were first sterilized for 15 min with UV-C (254 nm) radiation with a low-pressure Hg lamp, placed at the bottom of a well plate (2 cm² diameter/well), and covered with 1 mL ~5 × 10⁶ PFU(CFU)/mL of the surrogate organism in PBS. After illumination for 90 min, organisms were retrieved by washing the films and wells with 1 mL PBS, followed by bath sonication (Branson 3800; 40 kHz) of films for 10 min in suspension. All microbial experiments were performed in duplicate, except for experiments used to determine kinetics in the presence/absence of 30 mM methanol and 100 mM L-histidine (sterile filtered), which were performed in triplicate.

RESULTS AND DISCUSSION

Physical, Optical, and Photothermal Properties. As synthesized Au nanocubes have a side length of 49 ± 4 nm, while Au nanorods have a length of 54 ± 3 nm and a diameter of 12 ± 1 nm (resulting in an aspect ratio of 4.4:1), as determined by analyzing TEM images (*Figures 1a–c*; averaged over 20 individual particle measurements). These results agree well with DLS analysis that indicate the hydrodynamic diameter

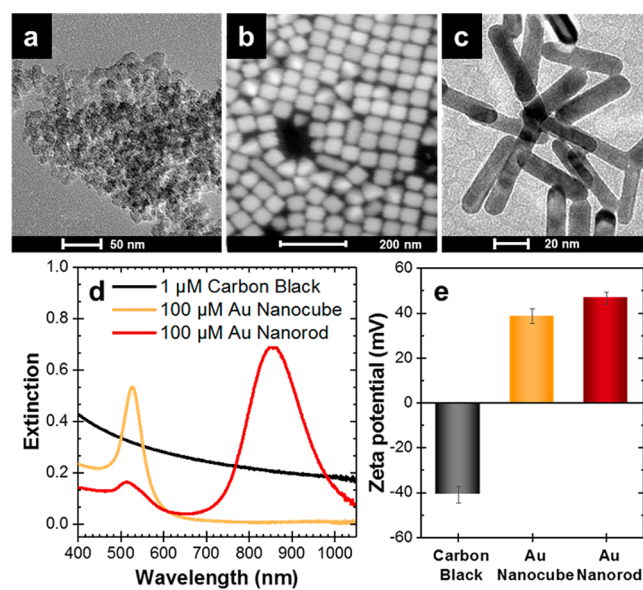


Figure 1. Photothermal nanomaterial characterization: (a) TEM of Carbon black, (b) SEM of Au nanocubes, (c) TEM of Au nanorods; (d) UV-vis extinction spectra of carbon black, Au nanocubes, and Au nanorods; and (e) PALS measurements of zeta-potential.

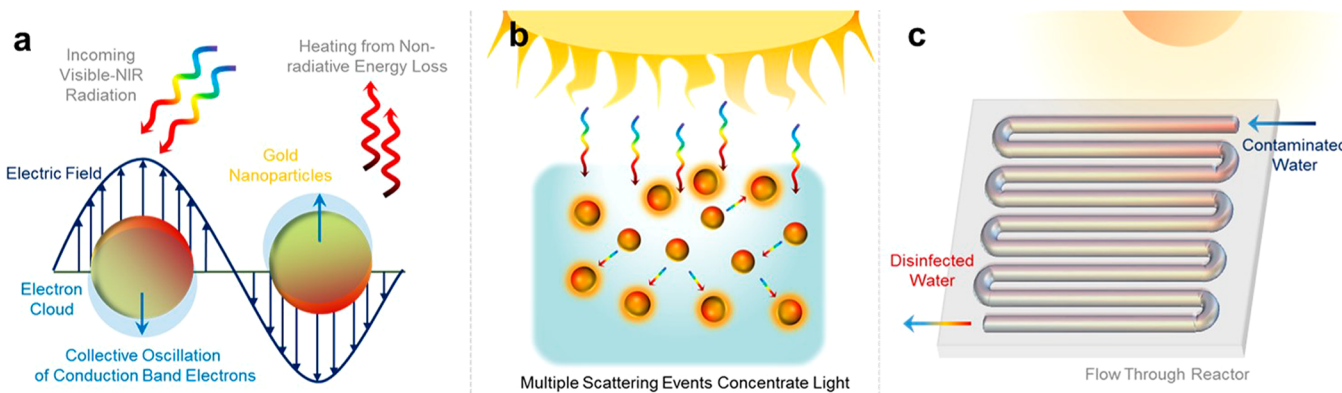


Figure 2. (a) Photothermal conversion mechanism for surface plasmonic Au nanoparticles. Incoming photons with a corresponding resonant frequency interact with an electric field surrounding the nanoparticle to produce a collective oscillation of conduction band electrons. Energy buildup at the surface of the particle is released in the form of heat, leading to high surface temperatures. (b) Under low-intensity noncoherent solar radiation, heat is generated through the concentration of light by multiple scattering events. (c) A possible photothermal material disinfection reactor schematic. Photothermal nanoparticles are coated inside a transparent substrate with a tortuous flow path employed to increase contact time. Compound parabolic reflectors, or other light concentrating features, could be used to increase solar radiation intensity.

of 51 ± 1 nm for Au nanocubes and 51 ± 3 nm for Au nanorods when dispersed in water. DLS correlation function curves (SI Figure S7) clearly indicate the two-phase anisotropic structure of Au nanorods, compared with Au nanocubes and carbon black. The size of individual particulate features within the carbon black structure was determined by TEM to be 14 ± 3 nm. However, as can be seen in Figure 1a, the primary features form larger agglomerates and/or aggregates. This corresponds well to DLS measurements, which report the hydrodynamic radius of carbon black as 163 ± 6 nm with a greater polydispersity index (PDI) of 0.3 compared to Au nanocubes (PDI = 0.07). Zeta potential measurements indicate that Au nanoparticles have a positive surface charge, $\zeta = 38.7 \pm 3.2$ mV and 46.8 ± 2.7 mV for cubes and rods, respectively, while carbon black has a negative surface charge of $\zeta = -41.0 \pm 3.6$ mV (Figure 1d). These values are expected, as CTAB bound to the surface of the Au nanoparticle imparts a positive surface charge,³⁵ while the negative surface charge on carbon black is likely to have been introduced during manufacturing to improve its water dispersivity.

Characteristic SPR absorption bands of as-synthesized Au nanoparticles are shown in Figure 1e. The location and intensity of absorption peaks of SPR materials are known to be dependent on composition, shape, and interparticle arrangement.^{27,36} Both Au nanocubes and nanorods exhibit an absorption peak at 530 nm, corresponding to the radial SPR band.³⁹ Au nanorods also have a large absorption peak in the NIR region at 875 nm, corresponding to the longitudinal (length-wise) SPR band.³⁷ These strong absorption bands result from the collective oscillation of unbound electrons in the conduction band, which creates an electric field around the particle that has resonant energies corresponding to visible and NIR wavelengths (Figure 2a).^{37,38} When enough photons are absorbed by the particle, hot electrons are promoted high into the conduction band where the energy levels are distributed nonthermally, preventing radiative escape.³⁹ Energy is then quickly redistributed among many lower energy electrons allowing greater phonon interactions which transfer energy to the crystal lattice, and subsequently into the surrounding environment, as heat.⁴⁰ In contrast, Emperor 2000 carbon black absorbs photons over a very broad range of wavelengths without presenting a specific absorption maxima; therefore it

has no occurrence of SPR, but can produce high temperatures through the localized heating of broad-band light absorbing particles.

The photothermal properties of these materials were confirmed by monitoring the increase in bulk temperature under simulated solar radiation, as shown in Figure 3. Figures 3a and b compare the temperature increase for each material at the same molar concentration. Results indicate that carbon black is the most efficient photothermal converter in terms of bulk water heating, reaching a temperature 5.6°C higher than DI water alone after 30 min irradiation. When a 675 nm long-

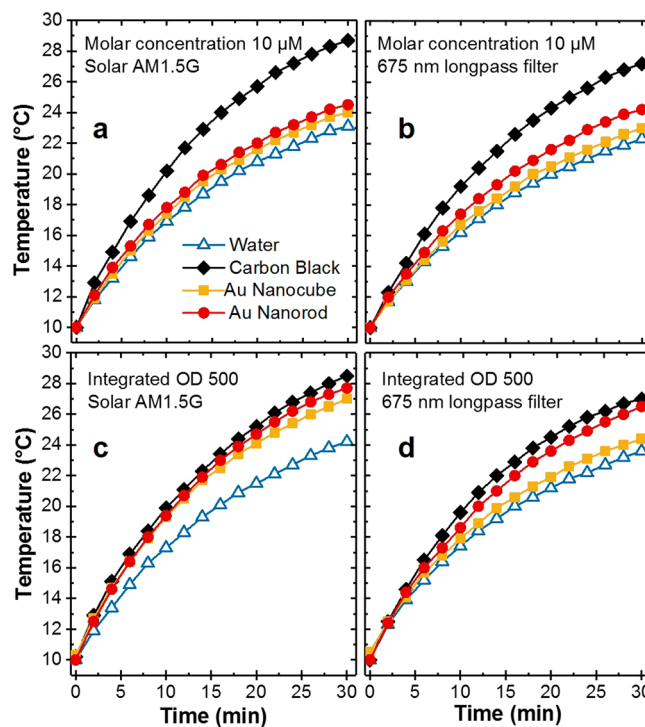


Figure 3. Bulk temperature increase for each photothermal material normalized for mass concentration ($10 \mu\text{M}$) under (a) 1 sun irradiation, (b) 1 sun irradiation with a 675 nm long-pass filter; and normalized for optical density (OD 500) under (c) 1 sun irradiation, (d) 1 sun irradiation with a 675 nm long-pass filter.

pass filter was employed to observe the impact of longer NIR wavelengths, overall temperature increase was reduced for all photothermal materials. Noticeably, the Au nanocube temperature increase was reduced by a proportionally larger amount, compared with Au nanorod and carbon black, resulting in a temperature increase negligibly greater than DI water alone. Considering the absorption spectra of each material, Au nanocubes absorb very little radiation at wavelengths longer than 675 nm, explaining their poor photothermal performance with NIR wavelengths. Figures 3c and d compare the temperature increase for each material at the same optical density, varying the concentration to allow normalization by the total number of photons absorbed between 300 and 1000 nm. At the same optical density, the heat conversion efficiency is found to be almost the same for all three photothermal materials. This supports the assertion that the amount of heat produced within the system under solar radiation conditions is closely correlated to the number of photons absorbed and the material's ability to absorb the most abundant solar wavelengths.

Inactivation Kinetics. Results for the solar light induced photoinactivation of *E. coli* K-12, MS2, and PR772 are shown in Figure 4. *E. coli* was the most susceptible to inactivation with Au nanoparticles, resulting in >5-log inactivation with both Au nanocubes and nanorods within 60 min simulated solar radiation. PR772 was the most resistant to inactivation with Au nanorods, resulting in 1.6 log-inactivation after 100 min of radiation (compared with 1.1 log-inactivation in the dark). For all materials and microorganisms tested, inactivation occurred more quickly when exposed to simulated solar radiation, compared to the associated dark control. However, removal in the dark was also observed, particularly in the presence of Au nanorods, which were able to completely remove *E. coli* without the assistance of light. We attribute this result to the presence of a bound layer of CTAB on the surface of the Au nanoparticles.³⁵ CTAB is a cationic surfactant utilized in the synthesis of Au nanoparticles to control growth and is essential to prevent particles from coalescing and precipitating out of solution, but is known to have antimicrobial and cytotoxic properties through detergency and the breaking up of cell membrane bilayers.^{41–43} This biocidal capability of nanoparticle bound CTAB against *E. coli* has been previously demonstrated using 10 nm Fe₃O₄ spheres at concentrations as low as 0.1 g/L (with 1.5% (wt) CTAB).⁴⁴ Bacteriophage, alternatively, are not reported to have a strong biocidal response at the concentration of CTAB predicted in our 25 μM Au nanoparticle suspension (<0.1 mM).^{35,45} This assertion is supported by dark controls using the carbon black which did not show appreciable inactivation for *E. coli* or MS2. The higher levels of dark removal resulting from Au nanorod exposure, compared to Au nanocubes, could be explained by greater surface area, which would result in higher amounts of CTAB at the same Au molar concentrations. The lack of Au nanocube aggregation under the same experimental condition (DLS analysis; results not shown) excluded the potential contribution of released CTAB to observed inactivation.

Although carbon black was determined to be the most efficient photothermal converter for increasing bulk temperature, it was largely ineffective for inactivating *E. coli* and bacteriophage MS2. Recalling that solar heat generation in photothermal nanoparticles relies on localized heating in a small spatial domain, it follows that effective inactivation would require close interaction between the nanoparticle and the

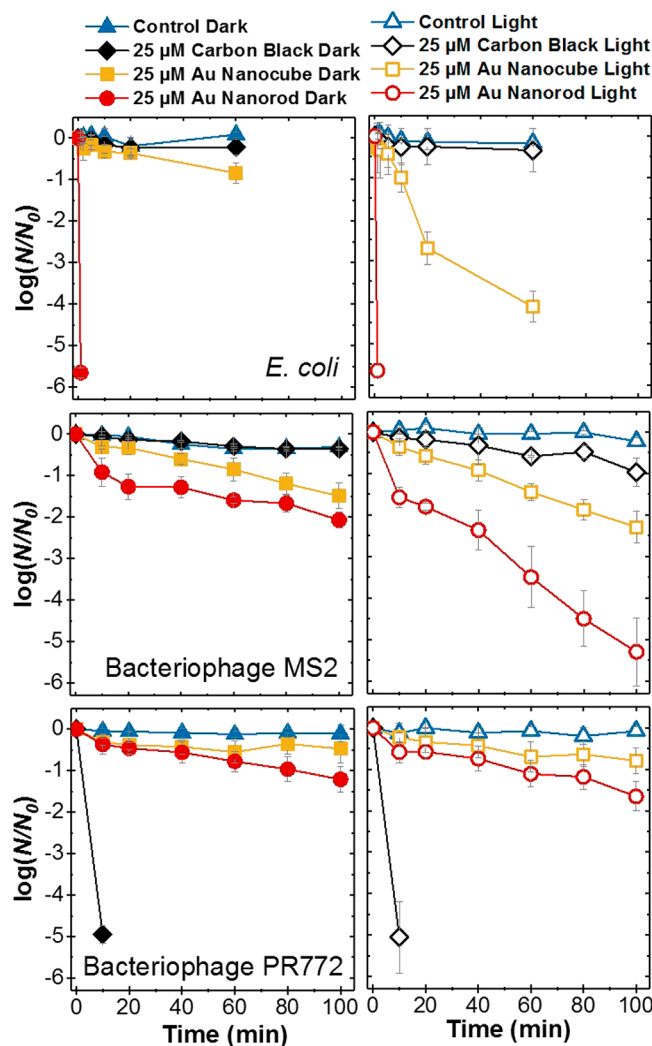


Figure 4. Inactivation of *E. coli* K-12, bacteriophage MS2, and bacteriophage PR772 in the dark (filled marker) and under simulated solar radiation (open marker) with no photothermal material (blue triangle), carbon black (gray diamond), Au nanocube (yellow square), Au nanorod (red circles).

microorganism. All surrogates used in this study are reported to be negatively charged in water (*E. coli* $\zeta \approx -42$ mV,⁴⁶ MS2 $\zeta \approx -18$ mV,⁴⁷ PR772 $\zeta \approx -9.5$ mV⁴⁸); therefore, the high negative surface charge of carbon black may impede close interaction between organism and nanoparticle. To this same end, the highly positive surface charge of Au nanoparticles infers an advantage for inactivation of *E. coli* and MS2 by drawing the organism close to particle; indeed the use of CTAB or other quaternary amine surface groups has previously been employed for the successful electrostatic capture of *E. coli* and MS2 bacteriophage.^{44,49}

Surprisingly, PR772 results indicated a > 5-log removal after less than 30 s in the presence of carbon black. However, unlike *E. coli* when exposed to Au nanorods, complete inactivation of PR772 with carbon black in the dark was not achieved: after the initial ~5-log removal, 0–10 colonies remained present on both the zero and 10-fold dilution plates, while complete inactivation (zero colonies without dilution) was achieved in the light. This indicates that PR772 is being removed from solution primarily by an adsorption mechanism, rather than through photothermal inactivation. The surface of PR772 contains apical spike

proteins, while MS2 is a spherical virion with capsid protein dimers and a single maturation protein. These surface spike proteins on PR772 are employed by the bacteriophage for attachment to the host cell.⁵⁰ It is posited that these proteins may be involved in a surface interaction with carbon black. The variable responses of each surrogate to the same nanomaterial under the same experimental conditions highlights the need for current lab-scale research, especially those proposing to use newly developed materials with novel inactivation mechanisms, to validate any new technology with a wide range of surrogates and test organisms.

Many metallic and semimetallic nanoparticles can also produce reactive oxygen species (ROS) when exposed to solar radiation. Particularly, some noble metals exhibiting SPR have been shown to produce singlet oxygen (${}^1\text{O}_2$) through the transfer of energy from excited resonant hot electrons to absorbed molecular oxygen, although the quantum yield of this process for Au tends to be very low (0.006)⁵¹ and the effective absorption of O_2 strongly depends on the exposed facets of the nanomaterial.⁵² To study the effect of ROS on inactivation kinetics, MS2 inactivation experiments with Au nanorods were repeated in the presence of 30 mM methanol and 100 mM L-histidine, as shown in Figure 5. Methanol is a well-known

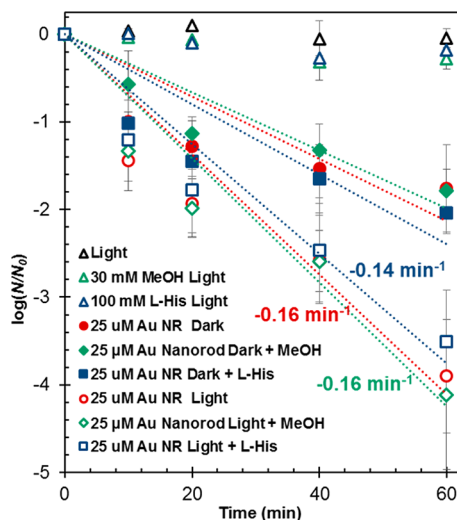


Figure 5. Inactivation of bacteriophage MS2 with Au nanorods in PBS (red circles) and in the presence of 30 mM methanol (green diamonds) and 100 mM L-histidine (blue squares) as ROS scavengers. Inactivation kinetics calculated using the standard Chick–Watson model.

scavenger of oxidative holes (h^+) and $\bullet\text{OH}$,⁵³ while L-histidine is a scavenger of ${}^1\text{O}_2$.⁵⁴ Inactivation rate constants were calculated using the standard Chick–Watson kinetic model, $\ln\left(\frac{N}{N_0}\right) = -kt$. Calculated rate constants showed no effect in the presence of methanol, and a small decrease in the presence of L-histidine. Although the difference in rate constant with the addition of L-histidine is negligible within a reasonable error range, the decrease was consistent within individual trials. While the presence of small amounts of ${}^1\text{O}_2$ cannot be entirely precluded, determined kinetics in the presence/absence of scavengers combined with the observed photothermal properties of these materials, provides strong support that inactivation indeed primarily occurs through a photoinitiated heat treatment mechanism.

Development of Photothermal Films. When photothermal materials are immobilized onto surfaces, the need to precipitate or filter them out is obviated, allowing for the design of flow-through reactors, such as the simple conceptual design represented in Figure 2c. We achieved the fabrication of photothermal films on transparent glass substrates as shown in Figure 6. Surface silanation was selected for its flexibility,

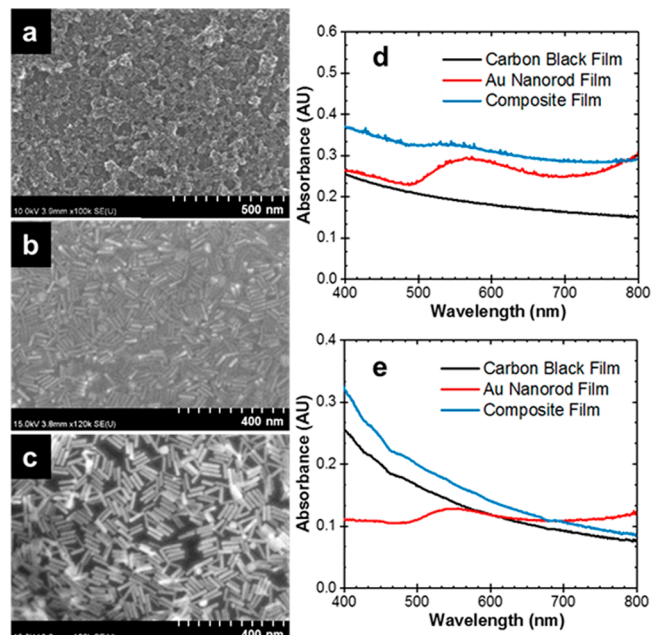


Figure 6. (a–c) SEM images of photothermal films fabricated on silicon by immobilization on a surface silane layer. (a) Carbon black films immobilized on APTMS; (b) Au nanorod films immobilized on MPTMS, and (c) Composite Au nanorod–carbon black films formed through layered application of carbon black on APTMS and Au nanorods on MPTMS. (d–e) Characterization of photothermal films immobilized on glass substrates by (d) UV–vis spectroscopy identifying the presence of SPR peaks in the Au NR and composite films, and (e) diffuse reflectance spectroscopy. DRS analyzes diffuse reflectance, accounting for scatter and providing a more accurate baseline.

allowing for the attachment of particles with varying surface properties by employing silanes with different terminal functional groups, in this case $-\text{NH}_2$ for carbon, and $-\text{SH}$ for Au. The effectiveness of surface silanation on both glass and carbon substrates also allows for the facile fabrication of composite films by the layered application of carbon black on APTMS, following by Au nanorods on MPTMS. Carbon black nanoparticles were able to form dense robust layers on APTMS-treated glass by straightforward drop-casting, however, initial attempts to perform similar procedures using Au nanorods resulted in highly monodispersed films (surface coverage $0.3 \pm 0.2\%$) with interparticle spacing several times the length of the particle itself. Such films are clearly nonideal for surface inactivation experiments in which close interaction between the particle and the virus is desired. By trapping the Au nanorods at a liquid–liquid interface and depositing them on an MPTMS-modified substrate, we were able to vastly improve the packing density of Au nanorods on glass, increasing it to $91 \pm 2\%$, as seen in Figure 6b, with the UV–vis spectra shown in Figure 6d.

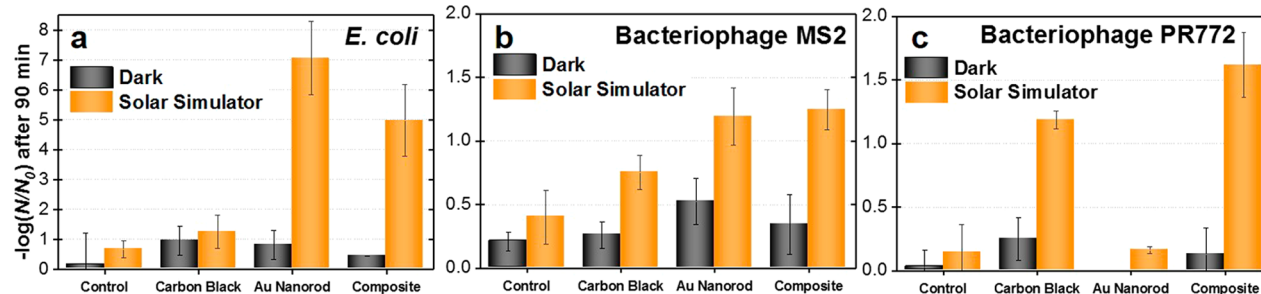


Figure 7. Inactivation of *E. coli* K-12, bacteriophage MS2, and bacteriophage PR772 after 90 min of 1 sun radiation.

In the UV-vis spectra, the characteristic Au nanorod peak near 530 nm is evident in both the Au nanorod film and composite film samples. The absorption spectrum of the Au nanorod film is considerably broadened, compared with the particles in solution. The peak absorption wavelength of materials exhibiting SPR can be manipulated by the connections between particles, referred to as hotspots.⁵⁵ These hotspots allow electron transfer between particles, creating new modes of plasmonic oscillation at new characteristic frequencies. The disordered packing of nanorods on the surface thereby creates many different SPR modes based on the different orientations and connections between particles. As such, Au nanorod films fabricated through this method have two major advantages: (1) greatly reducing void spaces between particles, increasing the likelihood of interaction with microorganisms, and (2) broadening the absorption spectrum of the material, increasing the useful number of photons in the solar spectrum. Films were also characterized by DRS, with results shown in Figure 6e. Due to the different reflection and scattering properties of these films, UV-vis spectroscopy may not be able to accurately capture the relative magnitude of absorption for each film, although the shape of the absorption spectrum is preserved. By controlling for both specular and diffuse reflection, DRS results were able to more reliably show the overall increase in absorption for composite films, compared with carbon black or Au nanorods alone.

Surface Inactivation. The disinfection capacity of photothermal films was studied using *E. coli* K-12, MS2, and PR772 by covering films with a shallow layer (1 mL, < 1 cm depth) of PBS containing $\sim 5 \times 10^6$ PFU(CFU)/mL and exposing the material to simulated solar radiation at an intensity of 1 sun. Results of 90 min inactivation with each material and organism are shown in Figure 7. Based on the results in suspension, the aim in fabricating composite films was to improve inactivation performance against all organisms, while reducing the amount of Au required in the fabrication process. Au nanorod films were the most effective for inactivating *E. coli*, while Au nanorod and composite films performed equally well with MS2, and the composite and carbon black films performed the best against PR772. Composite films fabricated through the layered deposition of densely packed Au nanorod islands on a carbon black coated substrate were the most broadly effective material, able to achieve a 5-log inactivation of *E. coli*, and a 1.3 and 1.6-log inactivation of MS2 and PR772, respectively, in 90 min illumination.

The surface inactivation experiments herein represent the first application of solar-activated (i.e., under low-intensity, noncoherent radiation) photothermal materials in an immobilized configuration for the direct thermal inactivation of microorganisms in water. As with any disinfection technology,

variation in rate of inactivation between different organisms is reported, however, thermal methods are seemingly effective against the vast majority of pathogens of concern, including those with notable resistances to other treatment methods such as *Cryptosporidium parvum* and *Pseudomonas aeruginosa* resistance to chlorination, and bacteriophage MS2 resistance to UV-C light treatment.^{56–61} Results from this study indicate that although the use of photothermal nanomaterials for direct thermal inactivation can be effective against the bacteria and viruses with different properties tested in this study, optimizing the close-range interaction between the heat-generation source and microorganisms is an important parameter to consider, since, unlike bulk water heating, heat transfer from photothermal material to target pathogen depends on this close-range interaction. Beyond a simple positively charged surface, such as a cationic surfactant bilayer, more selective functionalization might be desired as natural organic matter present in surface waters could easily foul a positively charged surface and interfere with such interactions.^{62–64} In addition, the heat gradients within the solar-activated nanoparticle suspension are highly heterogeneous,^{24,25} requiring more complex methods of nanoscale temperature measurement in order to determine a direct kinetic relationship between heat generation and inactivation. This heterogeneous heating is known to produce steam and water vapor; the role that phase changes within a small spatial domain may play in microbial inactivation is likewise unknown.

While the required time for inactivation of surrogates tested in this proof-of-concept study remains relatively long, there exists ample opportunity to improve the efficiency and performance of photothermal materials by developing methods to more accurately monitor nanoscale temperature increase and designing selective surface functionalization to draw microorganisms close to the particle for more efficient heat transfer. Pending future increases in photon-to-localized heat conversion efficiency, establishment of more detailed kinetic relations, and fabrication of thin-channel, flow-through reactors with surface immobilization; photothermal materials have the potential to provide a new and innovative method for solar disinfection, able to harness a greater fraction of solar wavelengths than any currently developed material-based solar water treatment system.

ASSOCIATED CONTENT

Supporting Information

This material is available free of charge via the Internet at <https://pubs.acs.org>. The Supporting Information is available free of charge on the ACS Publications website at DOI: [10.1021/acs.est.7b04442](https://doi.org/10.1021/acs.est.7b04442).

Additional material available in the Supporting Information as cross-referenced throughout ([PDF](#))

AUTHOR INFORMATION

Corresponding Author

*Phone: +1-203-432-4386; e-mail: jaehong.kim@yale.edu.

ORCID

Jae-Hong Kim: [0000-0003-2224-3516](#)

Notes

The authors declare no competing financial interest.

ACKNOWLEDGMENTS

This work was partly supported by the NSF Nanosystems Engineering Research Center for Nanotechnology-Enabled Water Treatment (ERC-1449500). Support for S.L. was provided by the Natural Sciences and Engineering Research Council of Canada. We thank Professor Qilin Li and Professor Naomi Halas at Rice University for valuable discussion in the ideation and planning phase of this project.

REFERENCES

- (1) Ghebreyesus, T. A.; Lake, A.; Grojec, A. *Progress on Drinking Water, Sanitation and Hygiene: 2017 Update and SDG Baselines*; Report for the World Health Organization (WHO) and the United Nations Children's Fund (UNICEF) joint monitoring programme for water supply and sanitation: Geneva, Switzerland, 2017; pp 1–110.
- (2) Meierhofer, R.; Wegelin, M. *Solar Water Disinfection: A Guide for the Application of SODIS*; Report No 06/02 for Water & Sanitation in Developing Countries (SANDEC) at the Swiss Federal Institute for Environmental Science and Technology (EAWAG): Dübendorf, Switzerland, 2002; pp 1–88.
- (3) Dejung, S.; Fuentes, I.; Almanza, G.; Jarro, R.; Navarro, L.; Arias, G.; Urquiza, E.; Torrico, A.; Fernandez, W.; Iriarte, M.; Birrer, C.; Stahel, W. A.; Wegelin, M. Effect of solar water disinfection (SODIS) on model microorganisms under improved and field SODIS conditions. *Aqua* **2007**, *56* (4), 245–256.
- (4) Fisher, M. B.; Iriarte, M.; Nelson, K. L. Solar water disinfection (SODIS) of *Escherichia coli*, *Enterococcus spp.*, and MS2 coliphage: Effects of additives and alternative container materials. *Water Res.* **2012**, *46* (6), 1745–1754.
- (5) Loeb, S.; Hofmann, R.; Kim, J. H. Beyond the pipeline: Assessing the efficiency limits of advanced technologies for solar water disinfection. *Environ. Sci. Technol. Lett.* **2016**, *3* (3), 73–80.
- (6) Fewtrell, L.; Kaufmann, R. B.; Kay, D.; Enanoria, W.; Haller, L.; Colford, J. M., Jr. Water, sanitation, and hygiene interventions to reduce diarrhoea in less developed countries: a systematic review and meta-analysis. *Lancet Infect. Dis.* **2005**, *5* (1), 42–52.
- (7) McGuigan, K. G.; Conroy, R. M.; Mosler, H. J.; du Preez, M.; Ubomba-Jaswa, E.; Fernandez-Ibanez, P. Solar water disinfection (SODIS): a review from bench-top to roof-top. *J. Hazard. Mater.* **2012**, *235–236*, 29–46.
- (8) Bursill, L. A.; Stadelmann, P. A.; Peng, J. L.; Prawer, S. Surface plasmon observed for carbon nanotubes. *Phys. Rev. B: Condens. Matter Mater. Phys.* **1994**, *49* (4), 2882–2887.
- (9) Nikitin, A. Y.; Guinea, F.; Garcia-Vidal, F. J.; Martin-Moreno, L. Surface plasmon enhanced absorption and suppressed transmission in periodic arrays of graphene ribbons. *Phys. Rev. B: Condens. Matter Mater. Phys.* **2012**, *85* (8), 081405.
- (10) Jiang, R. B.; Cheng, S.; Shao, L.; Ruan, Q. F.; Wang, J. F. Mass-based photothermal comparison among gold nanocrystals, PbS nanocrystals, organic dyes, and carbon black. *J. Phys. Chem. C* **2013**, *117* (17), 8909–8915.
- (11) Mansour, K.; Soileau, M. J.; Vanstryland, E. W. Nonlinear optical-properties of carbon-black suspensions (ink). *J. Opt. Soc. Am. B* **1992**, *9* (7), 1100–1109.
- (12) Guo, C. F.; Sun, T.; Cao, F.; Liu, Q.; Ren, Z. Metallic nanostructures for light trapping in energy-harvesting devices. *Light: Sci. Appl.* **2014**, *3* (4), e161.
- (13) Govorov, A. O.; Zhang, W.; Skeini, T.; Richardson, H.; Lee, J.; Kotov, N. A. Gold nanoparticle ensembles as heaters and actuators: melting and collective plasmon resonances. *Nanoscale Res. Lett.* **2006**, *1* (1), 84–90.
- (14) Govorov, A. O.; Richardson, H. H. Generating heat with metal nanoparticles. *Nano Today* **2007**, *2* (1), 30–38.
- (15) Lukianova-Hleb, E.; Hu, Y.; Latterini, L.; Tarpani, L.; Lee, S.; Drezek, R. A.; Hafner, J. H.; Lapotko, D. O. Plasmonic nanobubbles as transient vapor nanobubbles generated around plasmonic nanoparticles. *ACS Nano* **2010**, *4* (4), 2109–2123.
- (16) Chen, X.; Chen, Y.; Yan, M.; Qiu, M. Nanosecond photothermal effects in plasmonic nanostructures. *ACS Nano* **2012**, *6* (3), 2550–2557.
- (17) Santos, G. M.; Ferrara, F. I. D.; Zhao, F. S.; Rodrigues, D. F.; Shih, W. C. Photothermal inactivation of heat-resistant bacteria on nanoporous gold disk arrays. *Opt. Mater. Express* **2016**, *6* (4), 1217–1229.
- (18) Jo, W.; Kim, M. J. Influence of the photothermal effect of a gold nanorod cluster on biofilm disinfection. *Nanotechnology* **2013**, *24* (19), 195104.
- (19) Turcheniuk, K.; Turcheniuk, V.; Hage, C. H.; Dumych, T.; Bilyy, R.; Bouckaert, J.; Heliot, L.; Zaitsev, V.; Boukherroub, R.; Szunerits, S. Highly effective photodynamic inactivation of *E. coli* using gold nanorods/SiO₂ core-shell nanostructures with embedded verteporfin. *Chem. Commun.* **2015**, *51* (91), 16365–16368.
- (20) Castillo-Martinez, J. C.; Martinez-Castanon, G. A.; Martinez-Gutierrez, F.; Zavala-Alonso, N. V.; Patino-Marin, N.; Nino-Martinez, N.; Zaragoza-Magana, V.; Cabral-Romero, C. Antibacterial and antibiofilm activities of the photothermal therapy using gold nanorods against seven different bacterial strains. *J. Nanomat.* **2015**, *783671*, 1–7.
- (21) Zhu, Y.; Ramasamy, M.; Yi, D. K. Antibacterial activity of ordered gold nanorod arrays. *ACS Appl. Mater. Interfaces* **2014**, *6* (17), 15078–15085.
- (22) Carlson, M. T.; Green, A. J.; Richardson, H. H. Superheating water by continuous wave excitation of gold nanodots. *Nano Lett.* **2012**, *12* (3), 1534–1537.
- (23) Roper, D. K.; Ahn, W.; Hoepfner, M. Microscale heat transfer transduced by surface plasmon resonant gold nanoparticles. *J. Phys. Chem. C* **2007**, *111* (9), 3636–3641.
- (24) Neumann, O.; Urban, A. S.; Day, J.; Lal, S.; Nordlander, P.; Halas, N. J. Solar vapor generation enabled by nanoparticles. *ACS Nano* **2013**, *7* (1), 42–49.
- (25) Hogan, N. J.; Urban, A. S.; Ayala-Orozco, C.; Pimpinelli, A.; Nordlander, P.; Halas, N. J. Nanoparticles heat through light localization. *Nano Lett.* **2014**, *14* (8), 4640–4645.
- (26) Fang, Z.; Zhen, Y. R.; Neumann, O.; Polman, A.; Garcia de Abajo, F. J.; Nordlander, P.; Halas, N. J. Evolution of light-induced vapor generation at a liquid-immersed metallic nanoparticle. *Nano Lett.* **2013**, *13* (4), 1736–1742.
- (27) Ni, W.; Kou, X.; Yang, Z.; Wang, J. Tailoring longitudinal surface plasmon wavelengths, scattering and absorption cross sections of gold nanorods. *ACS Nano* **2008**, *2* (4), 677–686.
- (28) Sun, Z.; Yang, Z.; Zhou, J.; Yeung, M. H.; Ni, W.; Wu, H.; Wang, J. A general approach to the synthesis of gold-metal sulfide core-shell and heterostructures. *Angew. Chem., Int. Ed.* **2009**, *48* (16), 2881–2885.
- (29) Nikoobakht, B.; El-Sayed, M. A. Preparation and growth mechanism of gold nanorods (NRs) using seed-mediated growth method. *Chem. Mater.* **2003**, *15* (10), 1957–1962.
- (30) Fabricius, A. L.; Duester, L.; Meermann, B.; Ternes, T. A. ICP-MS-based characterization of inorganic nanoparticles-sample preparation and off-line fractionation strategies. *Anal. Bioanal. Chem.* **2014**, *406* (2), 467–479.
- (31) Goss, C. A.; Charych, D. H.; Majda, M. Application of (3-mercaptopropyl)trimethoxysilane as a molecular adhesive in the

- fabrication of vapor-deposited gold electrodes on glass substrates. *Anal. Chem.* **1991**, *63* (1), 85–88.
- (32) Yun, S.; Park, Y. K.; Kim, S. K.; Park, S. Linker-molecule-free gold nanorod layer-by-layer films for surface-enhanced Raman scattering. *Anal. Chem.* **2007**, *79* (22), 8584–8589.
- (33) Kennedy, J. E., Jr.; Wei, C. I.; Oblinger, J. L. Methodology for enumeration of coliphages in foods. *Appl. Environ. Microbiol.* **1986**, *51* (5), 956–962.
- (34) Sanders, E. R. Aseptic laboratory techniques: plating methods. *J. Visualized Exp.* **2012**, No. 63, e3064.
- (35) Rosto-Kohanloo, B. C.; Bickford, L. R.; Payne, C. M.; Day, E. S.; Anderson, L. J. E.; Zhong, M.; Lee, S.; Mayer, K. M.; Zal, T.; Adam, L.; Dinney, C. P. N.; Drezek, R. A.; West, J. L.; Hafner, J. H. The stabilization and targeting of surfactant-synthesized gold nanorods. *Nanotechnology* **2009**, *20* (43), 434005.
- (36) Funston, A. M.; Novo, C.; Davis, T. J.; Mulvaney, P. Plasmon coupling of gold nanorods at short distances and in different geometries. *Nano Lett.* **2009**, *9* (4), 1651–1658.
- (37) Eustis, S.; El-Sayed, M. A. Why gold nanoparticles are more precious than pretty gold: Noble metal surface plasmon resonance and its enhancement of the radiative and nonradiative properties of nanocrystals of different shapes. *Chem. Soc. Rev.* **2006**, *35* (3), 209–217.
- (38) Halas, N. J.; Lal, S.; Chang, W. S.; Link, S.; Nordlander, P. Plasmons in strongly coupled metallic nanostructures. *Chem. Rev.* **2011**, *111* (6), 3913–3961.
- (39) Brongersma, M. L.; Halas, N. J.; Nordlander, P. Plasmon-induced hot carrier science and technology. *Nat. Nanotechnol.* **2015**, *10* (1), 25–34.
- (40) Watanabe, K.; Menzel, D.; Nilius, N.; Freund, H. J. Photochemistry on metal nanoparticles. *Chem. Rev.* **2006**, *106* (10), 4301–4320.
- (41) Simoes, M.; Pereira, M. O.; Vieira, M. J. Action of a cationic surfactant on the activity and removal of bacterial biofilms formed under different flow regimes. *Water Res.* **2005**, *39* (2–3), 478–486.
- (42) Lau, I. P.; Chen, H. J.; Wang, J. F.; Ong, H. C.; Leung, K. C. F.; Ho, H. P.; Kong, S. K. In vitro effect of CTAB- and PEG-coated gold nanorods on the induction of eryptosis/erythroptosis in human erythrocytes. *Nanotoxicology* **2012**, *6* (8), 847–856.
- (43) Nicoletti, G.; Boghossian, V.; Gurevitch, F.; Borland, R.; Morgenroth, P. The antimicrobial activity in vitro of chlorhexidine, a mixture of isothiazolinones ('Kathon'CG) and cetyltrimethyl ammonium bromide (CTAB). *J. Hosp. Infect.* **1993**, *23* (2), 87–111.
- (44) Jin, Y.; Deng, J.; Liang, J.; Shan, C.; Tong, M. Efficient bacteria capture and inactivation by cetyltrimethylammonium bromide modified magnetic nanoparticles. *Colloids Surf., B* **2015**, *136*, 659–665.
- (45) Ly-Chatain, M. H.; Moussaoui, S.; Vera, A.; Rigobello, V.; Demarigny, Y. Antiviral effect of cationic compounds on bacteriophages. *Front. Microbiol.* **2013**, *4* (46), 1–6.
- (46) Schwegmann, H.; Feitz, A. J.; Frimmel, F. H. Influence of the zeta potential on the sorption and toxicity of iron oxide nanoparticles on *S. cerevisiae* and *E. coli*. *J. Colloid Interface Sci.* **2010**, *347* (1), 43–48.
- (47) Redman, J. A.; Grant, S. B.; Olson, T. M.; Hardy, M. E.; Estes, M. K. Filtration of recombinant Norwalk virus particles and bacteriophage MS2 in quartz sand: Importance of electrostatic interactions. *Environ. Sci. Technol.* **1997**, *31* (12), 3378–3383.
- (48) Mesquita, M. M.; Stimson, J.; Chae, G. T.; Tufenkji, N.; Ptacek, C. J.; Blowes, D. W.; Emelko, M. B. Optimal preparation and purification of PRD1-like bacteriophages for use in environmental fate and transport studies. *Water Res.* **2010**, *44* (4), 1114–1125.
- (49) Snow, S. D.; Park, K.; Kim, J. H. Cationic fullerene aggregates with unprecedented virus photoinactivation efficiencies in water. *Environ. Sci. Technol. Lett.* **2014**, *1* (6), 290–294.
- (50) Saren, A. M.; Ravantti, J. J.; Benson, S. D.; Burnett, R. M.; Paulin, L.; Bamford, D. H.; Bamford, J. K. A snapshot of viral evolution from genome analysis of the tectiviridae family. *J. Mol. Biol.* **2005**, *350* (3), 427–440.
- (51) Gao, L.; Liu, R.; Gao, F.; Wang, Y.; Jiang, X.; Gao, X. Plasmon-mediated generation of reactive oxygen species from near-infrared light excited gold nanocages for photodynamic therapy in vitro. *ACS Nano* **2014**, *8* (7), 7260–7271.
- (52) Vankayala, R.; Kuo, C. L.; Sagadevan, A.; Chen, P. H.; Chiang, C. S.; Hwang, K. C. Morphology dependent photosensitization and formation of singlet oxygen (${}^1\Delta_g$) by gold and silver nanoparticles and its application in cancer treatment. *J. Mater. Chem. B* **2013**, *1* (35), 4379–4387.
- (53) Cho, M.; Chung, H.; Choi, W.; Yoon, J. Linear correlation between inactivation of *E. coli* and OH radical concentration in TiO₂ photocatalytic disinfection. *Water Res.* **2004**, *38* (4), 1069–1077.
- (54) Lee, J.; Mackeyev, Y.; Cho, M.; Li, D.; Kim, J.-H.; Wilson, L. J.; Alvarez, P. J. Photochemical and antimicrobial properties of novel C₆₀ derivatives in aqueous systems. *Environ. Sci. Technol.* **2009**, *43* (17), 6604–6610.
- (55) Lee, A.; Andrade, G. F.; Ahmed, A.; Souza, M. L.; Coombs, N.; Tumarkin, E.; Liu, K.; Gordon, R.; Brolo, A. G.; Kumacheva, E. Probing dynamic generation of hot-spots in self-assembled chains of gold nanorods by surface-enhanced Raman scattering. *J. Am. Chem. Soc.* **2011**, *133* (19), 7563–7570.
- (56) Ziembka, C.; Peccia, J. Net energy production associated with pathogen inactivation during mesophilic and thermophilic anaerobic digestion of sewage sludge. *Water Res.* **2011**, *45* (16), 4758–4768.
- (57) Pecson, B. M.; Martin, L. V.; Kohn, T. Quantitative PCR for determining the infectivity of bacteriophage MS2 upon inactivation by heat, UV-B radiation, and singlet oxygen: Advantages and limitations of an enzymatic treatment to reduce false-positive results. *Appl. Environ. Microbiol.* **2009**, *75* (17), 5544–5554.
- (58) Gomez-Couso, H.; Fontan-Sainz, M.; Ares-Mazas, E. Thermal contribution to the inactivation of *Cryptosporidium* in plastic bottles during solar water disinfection procedures. *Am. J. Trop. Med. Hyg.* **2010**, *82* (1), 35–39.
- (59) Spinks, A. T.; Dunstan, R. H.; Harrison, T.; Coombes, P.; Kuczera, G. Thermal inactivation of water-borne pathogenic and indicator bacteria at sub-boiling temperatures. *Water Res.* **2006**, *40* (6), 1326–1332.
- (60) Shrivastava, R.; Upadhyay, R. K.; Jain, S. R.; Prasad, K. N.; Seth, P. K.; Chaturvedi, U. C. Suboptimal chlorine treatment of drinking water leads to selection of multidrug-resistant *Pseudomonas aeruginosa*. *Ecotoxicol. Environ. Saf.* **2004**, *58* (2), 277–283.
- (61) Mamane, H.; Shermer, H.; Linden, K. G. Inactivation of *E. coli*, *B. subtilis* spores, and MS2, T4, and T7 phage using UV/H₂O₂ advanced oxidation. *J. Hazard. Mater.* **2007**, *146* (3), 479–486.
- (62) Li, D.; Lyon, D. Y.; Li, Q.; Alvarez, P. J. Effect of soil sorption and aquatic natural organic matter on the antibacterial activity of a fullerene water suspension. *Environ. Toxicol. Chem.* **2008**, *27* (9), 1888–1894.
- (63) Baalousha, M.; Manciulea, A.; Cumberland, S.; Kendall, K.; Lead, J. R. Aggregation and surface properties of iron oxide nanoparticles: Influence of pH and natural organic matter. *Environ. Toxicol. Chem.* **2008**, *27* (9), 1875–1882.
- (64) Collin, B.; Oostveen, E.; Tsypko, O. V.; Unrine, J. M. Influence of natural organic matter and surface charge on the toxicity and bioaccumulation of functionalized ceria nanoparticles in *Caenorhabditis elegans*. *Environ. Sci. Technol.* **2014**, *48* (2), 1280–1289.